Solubility of Nickel in Slags Equilibrated with Ni-S Melt

Hector M. Henao, Hino Mitsuhisa and Kimio Itagaki

Institute of Multidisciplinary Research for Advanced Materials (IMRAM)
Tohoku University
Katahira 2-1-1, Aoba-ku, Sendai, Miyagi 980-8577, Japan

ABSTRACT

To provide thermodynamic data for converting the nickel matte to liquid nickel, an experimental study was conducted in the phase equilibrium between the Ni-S melt and FeO_x-SiO_2, FeO_x-CaO or CaO-Al_2O_3 based slag melted in a magnesia crucible at 1773 and 1873 K. pSO_2 was controlled at 10.1 kPa while pO_2 and pS_2 ranged between those where NiO precipitated and Ni_3S_2 formed, respectively. The nickel content in the slag and the sulfur content in the metal at given pO_2 and pS_2 were smallest for the CaO-Al_2O_3 based slag. Both decreased with increasing temperature. At 1873 K, the content of nickel in the CaO-Al_2O_3 based slag at pO_2 of 10 Pa (near the precipitation of NiO) was 4%, while the content of sulfur in alloy is 0.4 mass %. Thus, the CaO-Al_2O_3 base slag at 1873 K would be suitable for direct converting of Ni_3S_2 to metallic nickel. The distribution behavior of nickel between the slag and the Ni-S melt was discussed based on the concept of oxidic and sulfidic dissolution.

1. INTRODUCTION

For the last forty years, the demand for nickel has grown at an annual rate of about 4%. In the long term, the demand is expected to remain at the same rate due to the growth in stainless steel demand and the need for advanced materials and alloys /1/. To meet the demands, development of new smelting and refining technologies is of practical importance.

The treatment of nickel sulfide ores consists of two stages of smelting and converting. The concentrates are oxidized to produce the Ni-Cu-S matte. The converting matte is separated into the sulfides of Ni_3S_2 and Cu_2S by the controlled slow cooling method. Mostly, Ni_3S_2 is converted to pure nickel or a nickel compound by hydrometallurgical processes. The alternative pyrometallurgical route to convert Ni_3S_2 to liquid nickel is employed in a process developed by INCO /2/, in which oxygen is injected in a top blown rotary converter (TBRC), followed by the reduction of nickel oxide formed during the blowing. A similar process developed by Ausmelt using a top submerged lancing process is reported by Robilliard et al. /3/.

To discuss the pyrometallurgical route for the conversion of Ni_3S_2 to liquid nickel from the standpoint of thermodynamics, equilibrium studies for the Ni-S and the slag or flux are of practical importance. Experimental works related to the phase equilibrium between the FeO_x-MgO-SiO_2 slag and the Ni_3S_2-FeS matte at 1523 K have been carried out by O'Connell and Toguri /4/ and Font et al. /5, 6/.

As a contribution to understanding the nickel smelting process and investigate new options for nickel smelting production, this paper evaluates the direct conversion of nickel sulfide to metallic nickel from the standpoint of thermodynamics at 1773 and 1873 K. As indicated schematically in Figure 1, the Ni-S alloy was equilibrated with the FeO_x-SiO_2, FeO_x-CaO or CaO-Al_2O_3 base slag under controlled partial pressures of S_2 and O_2. The partial pressure of SO_2 was controlled at 0.1 MPa by assuming that blowing air would oxidize the Ni-S melt. The sulfur and oxygen partial pressures ranged from that corresponding to the equilibrium with Ni_3S_2 to that near the precipitation of nickel oxide.

187
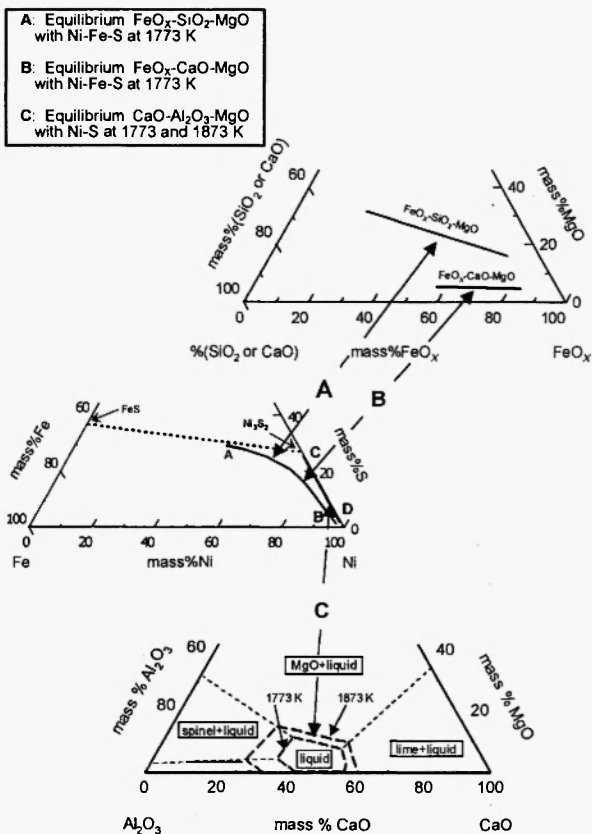
Fig. 1: Schematic diagrams equilibrium between Ni-Fe-S or Ni-S melt and slags.

2. EXPERIMENTAL

The furnace consists of a silicon carbide heating element and an alumina reaction tube. CO-CO_2-SO_2 gas mixtures with a flow rate regulated at 2.5×10^{-6} m^3/s were used to control the partial pressures of SO_2, O_2 and S_2. A CO gas train was equipped with soda lime and P_2O_5 columns to trap CO_2 gas and moisture, respectively, while CO_2 gas passed through a P_2O_5 column. The gas mixture was introduced into the reaction chamber through an alumina tube with an inner diameter of 6×10^{-4} m and a height of 0.6 m. The partial pressures of O_2, S_2 and SO_2 were calculated by using a ChemSage Ver. 4.20 software (GTT-Technologies, Aachen, Germany).

The experimental conditions are given in Table 1. The compositions of pre-melted slags are indicated in Table 2. 8 (eight) g of slag was equilibrated with the nearly equal amount of Ni-S in a magnesia crucible with

Table 1

Experimental conditions

Weights of Alloy and Slag	8 g
Equilibrium Time	36 h (1773 K) 24 h (1873 K)
Temperature	1773 K 1873 K
$\log pSO_2$ (oxidation of nickel matte with air) $1/2 S_2(gas) + O_2 (gas) = SO_2 (gas)$ $pSO_2 = (PSO_2/Pa)/(101325\ Pa)$	-1
Max. $\log pO_2$ (before solid NiO appears) $pO_2 = (PO_2/Pa)/(101325\ Pa)$	-5 (1773 K) -4 (1873 K)
Max. $\log pS_2$ (before Ni_3S_2 formation) $pS_2 = (PO_2/Pa)/(101325\ Pa)$	-0.9 (1773 K) -1.4 (1873 K)

Table 2

Composition (mass%) of pre-melted slags.

Component	FeO_x-CaO Slag 1773 K	FeO_x-SiO_2 Slag 1773 K	CaO-Al_2O_3 Slag 1773 and 1873K
FeO	70	67	-------
SiO_2	-------	33	-------
CaO	30	-------	49
Al_2O_3	-------	-------	51

an inner diameter of 1.1×10^{-2} m and a height of 5×10^{-2} m. Temperature of the sample was controlled by a SCR controller with a Pt/Pt-Rh thermocouple. Preliminary experiments have clarified that the equilibrium could be made in a restricted time of less than 100 ks by adjusting the sulfur content of starting alloy phase to be about 2 mass% smaller than the pre-estimated equilibrium value reported by Meyer et al./7/. The partial pressures are expressed as dimensionless ones defined in Table 1.

After equilibration, the sample was taken out of the furnace and quenched in a jet stream of argon or nitrogen. Specimens for the chemical analysis were prepared by

cutting the alloy sample into small pieces and grinding the slag sample, followed by thoroughly removing the small alloy particles included in the slag with a magnet. The slag and alloy specimens were analyzed by the inductively coupled plasma spectrometry (ICP) and by the conventional methods of chemical analysis with volumetric titration and gravity measurements. The total sulfur content in the slag specimen was determined by a combustion-infrared spectrometer (EMIA-580, HORIBA Co, Ltd., Kyoto, JAPAN).

3. RESULTS

3.1 Alloy Phase

3.1.1 Sulfur content

The relationships between the sulfur content in the alloy and log pS_2 or log pO_2 for both slag systems at 1773 and 1873 K are shown in Figures 2a and 2 b, respectively. The limits of pO_2 and pS_2, between which the experiments were carried out, are indicated with the dash-dot lines. At 1773 K, the right limit corresponds to the formation of Ni_3S_2 in the alloy phase, while the left limit to log pO_2 of -4.8 where the precipitation of solid NiO is anticipated. At 1873 K, the formation of Ni_3S_2 and the precipitation of solid NiO are anticipated at log pS_2 of -1.4 and log pO_2 of -4, respectively. Meyer *et al./7/* determined pS_2 in relation to the sulfur content in the Ni-S melt by equilibrating with H_2-H_2S gas mixtures, which is shown with a broken line in Figures 2a and 2b. It is found that the present results agree fairly well with the data by Meyer *et al./7/* within the scatter of the data even though the present system contains oxygen as a minor element and iron, which was introduced into the Ni-S melt from the iron containing slag. The figures also indicate that the content of sulfur in the Ni-S melt decreases with increasing temperature. The content of sulfur in the Ni-S melt near the anticipated precipitation of NiO is about 2 mass% and 0.4 mass% at 1773 and 1873 K, respectively.

3.1.2 Iron content

It was found that iron was introduced into the Ni-S melt from the FeO_x-SiO_2 and FeO_x-CaO based slags. The alloy composition for the equilibrium with FeO_x-SiO_2 and FeO_x-CaO based slags was plotted on the Ni-
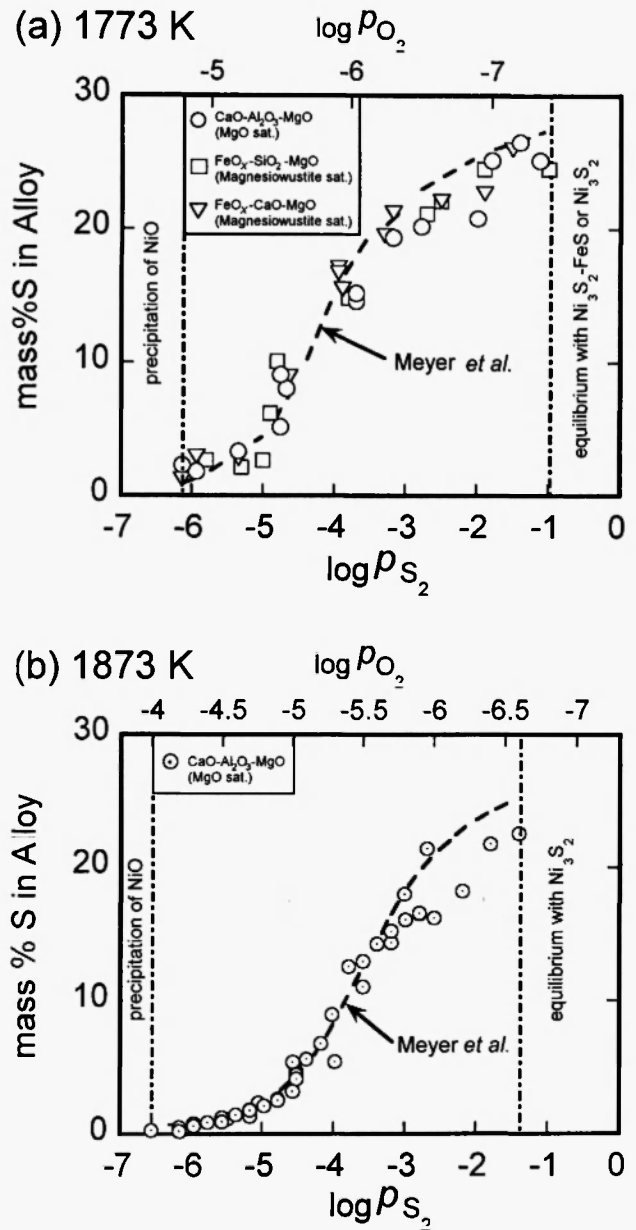
Fig. 2: Relationship between sulfur content in Ni-S or Ni-Fe-S melt and log pS_2 or log pO_2 in equilibrium with slags melted in MgO crucible at 1773 and 1873 K.

Fe-S ternary diagram in Figure 3 because the contents of other elements including oxygen are very small. It is shown that mass% of iron ranges between 1 and 25 mass% and that, at a given sulfur content, the iron content in the alloy equilibrating with the FeO_x-SiO_2 based slag is larger than that for the FeO_x-CaO based slag.

189
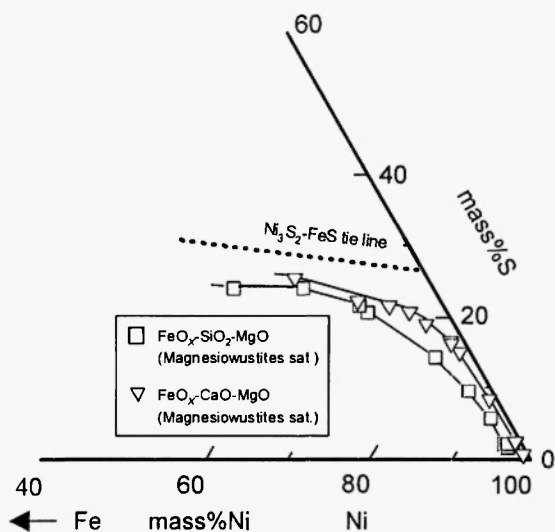
Fig. 3: Composition of Ni-Fe-S melts equilibrated with slags in MgO crucible at 1773 K.

3.2 Slag Phase

The slag compositions for the FeO$_X$-SiO$_2$-MgO or FeO$_X$-CaO-MgO slag are reproduced in Figure 4 on the A-B-C ternary diagram with a mass% scale where A corresponds to MgO, B to SiO$_2$ or CaO and C to (FeO$_X$+NiO). The solubility in the FeO$_X$-SiO$_2$ based slag is larger than that in the FeO$_X$-CaO based slag. Despite the presence of NiO, the liquidus line in the FeO$_X$-SiO$_2$ based slag is similar to that reported by Muan and Osborn/8/, which is very close to a tie line combining between FeO and MgO·SiO$_2$. It is reported by Johnson and Muan/9/ that the solubility of MgO in the FeO$_X$-CaO-MgO slag in coexistence with the solid magnesiowüstite changes very little with the FeO$_X$ content. This is in accordance with the present result.
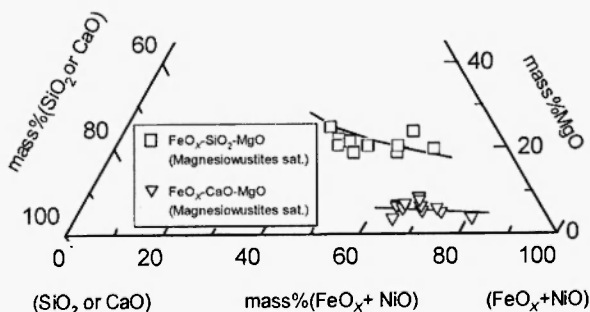
Fig. 4: Composition of slags equilibrated with Ni-Fe-S alloy melted in MgO crucible at 1773 K.

The composition of CaO-Al$_2$O$_3$ based slag is shown in Figure 5 on the MgO-NiO-(Al$_2$O$_3$+CaO) ternary diagram because the mass% ratio of CaO/Al$_2$O$_3$ is constant. It is indicated in the figure that the solubility of MgO in the slag decreases when the solubility of NiO increases. It is apparent that the MgO solubility increases with increasing temperature. The present experimental results agree with those reported in a reference/10/ when the content of MgO is extrapolated at the axis of MgO-(CaO+Al$_2$O$_3$).
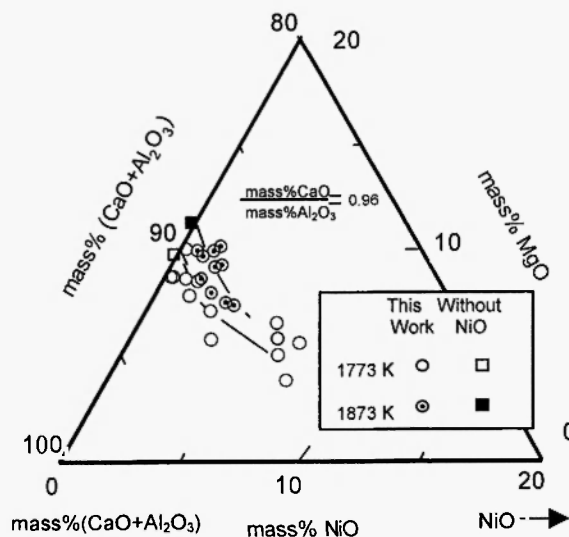
Fig. 5: Composition of CaO-Al$_2$O$_3$ based slag equilibrated with Ni-S alloy melted in MgO crucible at 1773 and 1873K.

3.2.1 Nickel content

The nickel content in the slags equilibrated with the Ni-S melt is plotted in Figure 6, in relation to log pO_2 or log pS_2. It is noted that the CaO-Al$_2$O$_3$ and FeO$_X$-SiO$_2$ based slags represent lower and higher solubility of nickel in the slag, respectively. The solubility of nickel in the FeO$_X$-SiO$_2$ based slag increases with increasing log pO_2 from 0.5 mass% at log pO_2 of -7.3 to 10 mass% at log pO_2 of -5.0. While, that in the FeO$_X$-CaO based slag decreases in a region of lower oxygen pressure from 6 mass% at log pO_2 of -7.1 to 4 mass% at log pO_2 of about -6.5, then, remarkably increases in the range of higher log pO_2 and becomes 20 mass% at log pO_2 of -4.8. It is shown that the nickel content in the CaO-Al$_2$O$_3$ based slag at 1773 K increases with increasing pO_2 from 0.3 mass% at log pO_2 of -7.3 to 5.7 mass% at log pO_2
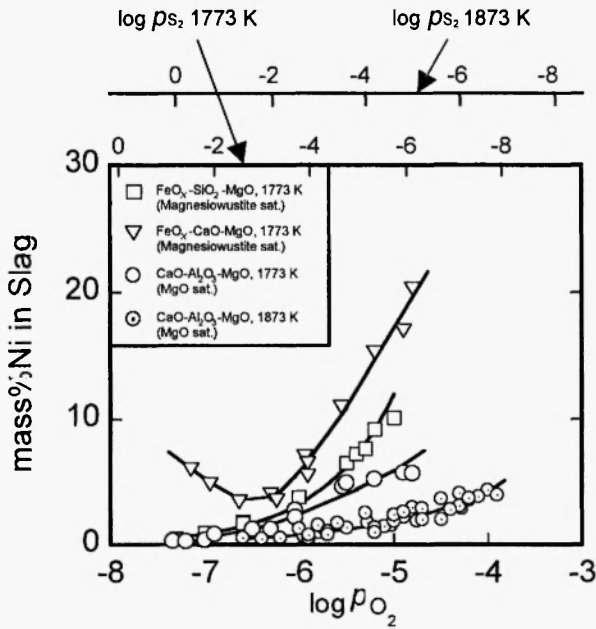
Fig. 6: Relationship between nickel content and log $pO2$ or log $pS2$ for slags melted in MgO crucible at 1773 and 1873 K.
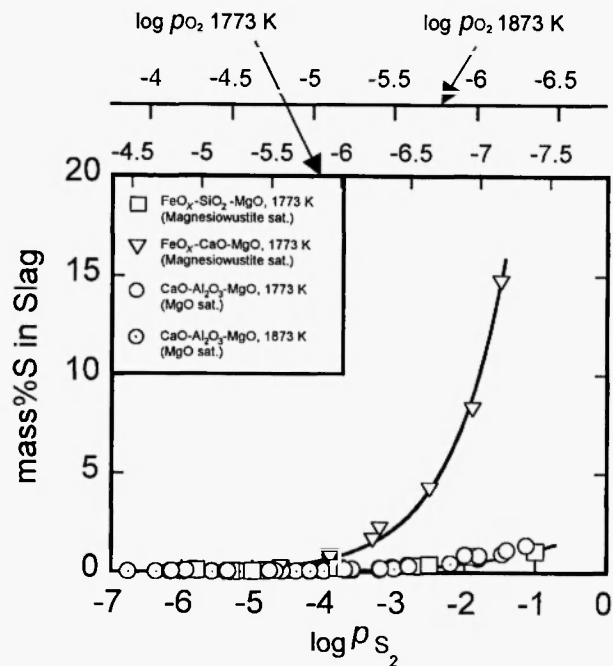
Fig. 7: Relationship between sulfur content and log $pS2$ or log $pO2$ for slags melted in MgO crucible at 1773 and 1873 K.

of -5.0. The figure also indicates that, for the CaO-Al_2O_3 based slag at a given pO_2, the content of nickel in the slag decreases when temperature is increased. At 1873 K the nickel content in the CaO-Al_2O_3 based slag increases from 0.3 mass% at log pO_2 of -6.6 to 4 mass% at log pO_2 of -4.0.

3.2.2 Sulfur content

The sulfur contents in the FeO$_\gamma$-CaO and FeO$_X$-SiO$_2$ based slags are shown in Figure 7, in relation to log pS_2 or log pO_2. It is noted that the solubility of sulfur is larger for the FeO$_X$-CaO based slag and shows comparable values for the FeO$_X$-SiO$_2$ and CaO-Al_2O_3 based slags. The solubility of sulfur in the CaO-Al_2O_3 based slag also shows small variation when temperature is increased.

4. DISCUSSION

4.1 Dissolution of Nickel in Slag

The dissolution of nickel and the activity coefficient of nickel oxide in the slags will be discussed on the basis of the distribution ratio of nickel between the slag

and alloy phases, which is defined by Eq. (1).

$$L_{Ni}^{s/Ni} = (mass\%Ni\ in\ slag)/\{mass\%Ni\ in\ alloy\} \quad (1)$$

When nickel is dissolved in the slag as an oxide, the distribution ratio can be analyzed thermo-dynamically on the basis of the following reaction to form a mono-metallic oxide,

$$Ni(l) + v/4\ O_2(g) = NiO_{v/2}\ (s) \quad (2)$$
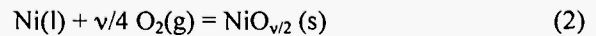
where the solid NiO$_{v/2}$ was taken as a reference of the NiO$_{v/2}$ activity for the lack in the thermodynamic data of the liquid NiO$_{v/2}$. The equilibrium constant of Eq. (2) is given by

$$K = a_{NiOv/2}/(\ a_{Ni}\ pO_2^{v/4}) \quad (3)$$

where a_{Ni} and $a_{NiOv/2}$ are activities of Ni and NiO$_{v/2}$, respectively. By combining Eqs. (1) and (3) and converting the mole fraction, N, in the activity relationship of $a = \gamma N$ with the Raoultian activity coefficient of γ into mass%, the following equation is

obtained.

$$\log L_{Ni}^{s/Ni} = \nu/4 \log pO_2 + \log\left[\{\gamma_{Ni}\}/(\gamma_{NiOv/2})\right]$$
$$+ \log\left[(n_T)/\{n_T\}\right] + \log K \qquad (4)$$

where, ( ) and { } denote the slag and alloy phases, respectively. n_T is the total number of moles in 100g of each phase, which was calculated on the mono-cation base.

$L_{Ni}^{s/Ni}$, which were obtained from the data on the nickel solubility obtained in the present study, are plotted in Figure 8 in relation to $\log pO_2$. For the FeO$_x$-SiO$_2$ and CaO-Al$_2$O$_3$ based slags, a nearly linear relationship is observed between $\log L_{Ni}^{s/Ni}$ and $\log pO_2$ with a gradient of about 1/2. This suggests that nickel dissolves in these slags as NiO, according to eq. (2) with $\nu = 2$. However, it is to be noted that the $L_{Ni}^{s/Ni}$ for the FeO$_x$-CaO based slag in the range of lower oxygen pressure decreases with increasing pO_2.
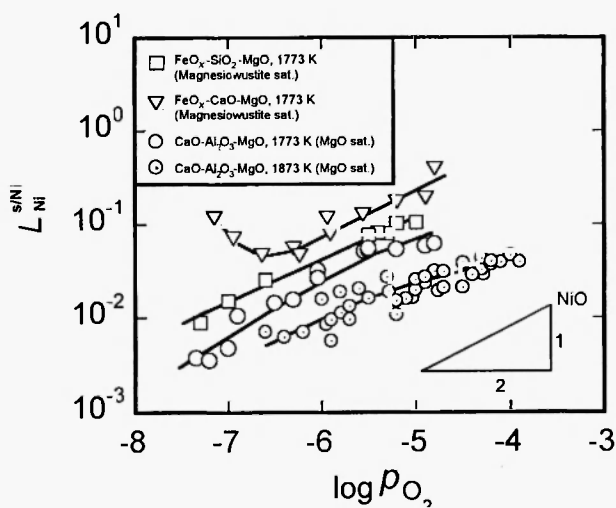
Fig. 8: Relationship between distribution ratio of nickel and log pO_2 for slags melted in MgO crucible at 1773 and 1873 K.

This anomalous behavior is considered to be ascribed to a mechanism of the nickel dissolution different from that of the dissolution as the oxide given by eq. (2). Owing to extremely large solubility of sulfur in this region for the FeO$_x$-CaO based slag, as shown in Figure 7, the dissolution of nickel as a sulfide may be suggested.

The linear relationship observed in Figure 8 suggests that the sum of activity coefficient ratio and n_T ratio in Eq. (4) does not change appreciably for each slag. Hence, the Raoultian activity coefficient of NiO in each slag can be calculated on the basic of Eq. (5)

$$Ni(l) + \tfrac{1}{2}O_2(g) = NiO (s) \qquad (5)$$
$$\Delta G^0/(J/mol) = -247750 + 92.52T/K$$
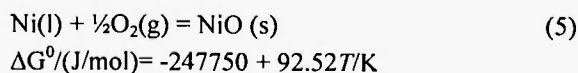
The standard free energy change and equilibrium constant of eq. (5) are given in a data book/11/. The Raoultian activity coefficient of nickel in the ternary Ni-Fe-S and binary Ni-S alloys, $\{\gamma_{Ni}\}$, is obtained from the data reported by Hsieh and Chang /12/ and J.M. Larrain /13/, respectively. The calculated γ_{NiO} are shown against $\log pO_2$ in Figure 9. In a general trend, the values for the CaO-Al$_2$O$_3$ and FeO$_x$-CaO based slags represent higher and lower γ_{NiO}, respectively. This trend may be mainly ascribed to a chemical property of NiO that is relatively neutral for the predominant slag components of basic CaO and MgO as well as acidic SiO$_2$. The Gibbs energy change of formation of 2MgO·SiO$_2$ is -18.8 kJ/mol of cation at 1773 K /14/. NiO and Al$_2$O$_3$ make a compound of NiO·Al$_2$O$_3$ with the Gibbs energy change of reaction of -6.9 kJ/mol of cation at 1773 K /15/, that is less negative than -9.1 kJ/mol of cation for NiO·Fe$_2$O$_3$ /16/. On the other hand, the chemical affinity between CaO and Al$_2$O$_3$ to make a compound of CaO·Al$_2$O$_3$ is
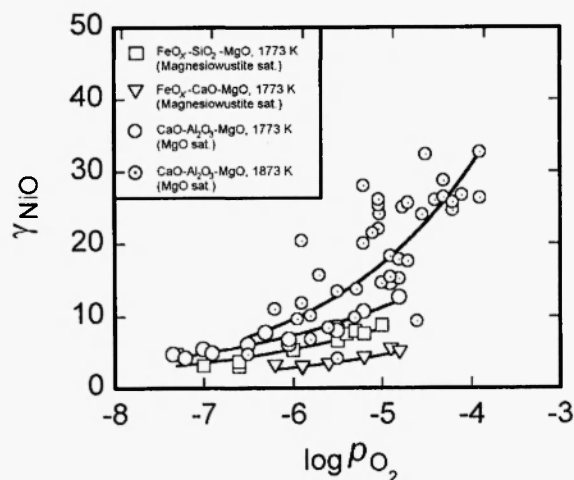
Fig. 9: Relationship between activity coefficient of NiO and log pO_2 for slags equilibrated with Ni-Fe-S or Ni-S melt at 1773 and 1873 K.

192

considered to be very large with the Gibbs energy change of reaction of -16.8 kJ/mol of cation at 1773 K /17/. Takeda and Yazawa /18/ suggested that a solution tends to repel the component which has a low affinity with the main components when these have a considerably high affinity to form the stable solution. The observed trend for γ_{NiO} is in concordance with this suggestion.

The experimental results for the solubility of nickel in the FeO_x-CaO based slag in the range of lower oxygen pressure, where log $L_{Ni}^{s/Ni}$ - log pO_2 plots deviate from the linear relationship, may be analyzed thermodynamically by combining the oxidic and sulfidic dissolution of nickel in the slag, (mass%Ni)$_{ox}$ and (mass%Ni)$_s$. According to Nagamori /19/, (mass%Ni)$_{ox}$ and (mass%Ni)$_s$ will be given by Eqs. (6) and (7), respectively.

$$(\text{mass\%Ni})_{ox} = A\; a_{Ni}\; pO_2^{1/2}/\gamma_{NiO} \tag{6}$$

$$(\text{mass\%Ni})_s = B\; a_{NiS}\; (\text{mass\%S}) \tag{7}$$

where A and B are constants. a_{NiS} is known from the data reported by Hsieh and Chang /12/ and the content of sulfur in the slag, (mass%S), was obtained in the present study. The present experimental data for the solubility of nickel in the FeO_x-CaO based slag were analyzed by regression on the basis of Eqs. (6) and (7). It was found that they could be reproduced well when A and B in eqs. (6) and (7) are 26000 and 6.4, respectively.

4.2 Application to Nickel Smelting

The nickel contents in the alloys equilibrated with the FeO_x-SiO$_2$ and FeO_x-CaO slags (fluxes) in a MgO crucible at 1773 K are relatively large at more than 95 mass%, but with considerable amounts of iron, sulfur and oxygen impurities. Thus, when a process of smelting the Ni-S or Ni-Fe-S alloy with the FeO_x-SiO$_2$ and FeO_x-CaO based slags (fluxes) is considered, a refining process for the metal product will be indispensable. Furthermore, it is to be noted that the content of nickel in the iron slag is considerably large at more than 10 mass%. This means that the loss of nickel in the slag will be substantial in the smelting process. A simple mass balance calculation was made by assuming smelting a matte with 50 mass% of nickel and 25

mass% of iron to produce a metallic phase with 2 mass% of iron and 2.5 mass% of sulfur and a slag phase with 40 mass% of iron. It is indicated that the losses of nickel in the FeO_x-SiO$_2$ and FeO_x-CaO based slag amount to 12 and 24 mass%, respectively. The loss of nickel would increase with increasing content of iron in the initial matte phase.

It was clarified in the present study that the content of nickel in the slag is not so high in the iron-free CaO-Al$_2$O$_3$ based slag. Furthermore, the amount of produced slag in the process would be kept small to reduce the loss of nickel in the slag. Thus, the present result suggests that the CaO-Al$_2$O$_3$ based slag will be more useful for converting the Ni-S melt to liquid nickel. The amounts of impurities such as sulfur and oxygen contained in the alloy equilibrated with the CaO-Al$_2$O$_3$ based slag can be reduced substantially by increasing the temperature from 1773 to 1873 K. Furthermore, it is to be noted that the content of nickel in the CaO-Al$_2$O$_3$ based slag is extremely small and decreases with increasing temperature. This means that the loss of nickel in the CaO-Al$_2$O$_3$ based slag can be kept down at a desired level if the amount of produced slag or used flux in the process is kept small and the process temperature is increased.

5. CONCLUSIONS

The main objective of the present study was to investigate and look for the slag or the flux suitable for direct converting of Ni$_3$S$_2$ to metallic nickel. Thus, the Ni-S alloy was equilibrated with the FeO_x-SiO$_2$, FeO_x-CaO or CaO-Al$_2$O$_3$ based slag in a magnesia crucible under controlled partial pressures of S$_2$ and O$_2$. The partial pressure of SO$_2$ was controlled at 0.1 MPa by assuming that blowing air would oxidize the Ni-S melt.

The obtained relationship between the contents of nickel in the slag and sulfur in the alloy, as shown in Figure 10, is helpful to summarize the experimental results. It is noted in general that the solubility of nickel in the slag increases when the content of sulfur in the alloy decreases. It is found that, for a given content of sulfur in the alloy, CaO-Al$_2$O$_3$ and FeO_x-CaO based slags represent lower and higher solubility of nickel in the slag, respectively. Figure 10 also indicates that the
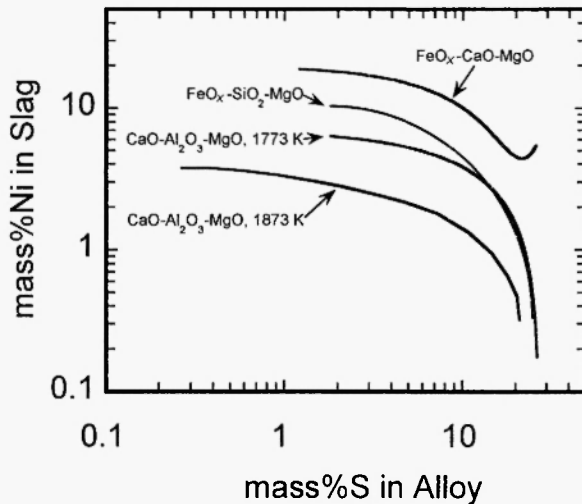
Fig. 10: Relationship between nickel content in slag and sulfur content in alloy for Ni-S melt equilibrated with slag.

nickel solubility in the $CaO-Al_2O_3$ based slag decreases with increasing temperature. The compositions of slag and alloy near the anticipated precipitation of NiO are indicated in Table 3. The contents of iron remaining in the alloy for the equilibrium with FeO_x-CaO or FeO_x-SiO_2 based slag are around 1 and 2%, respectively. In this condition, the content of nickel in the slag is higher than 10%. It is also indicated that further elimination of sulfur and oxygen from the nickel alloy is indispensable. However, the present results indicate that, by equilibrating the Ni-S melt with the $CaO-Al_2O_3$ based slag at 1873 K, the content of sulfur in the alloy is reduced considerably with an appreciable reduction in the solubility of nickel in the slag.

Table 3

Melt and slag composition at pO_2 just before precipitation of NiO.

Slag System	Nickel (mass%)		Slag (mass %)
	S	Fe	Ni
$FeO_x-CaO-MgO$, 1773 K	2	1	20
FeO_x-SiO_2-MgO, 1773 K	2	2	10
$Al_2O_3-CaO-MgO$, 1773 K	1	-	6
$Al_2O_3-CaO-MgO$, 1873 K	0.4	-	4

The behavior of nickel was discussed on the basis of the distribution ratio and analyzed thermo-dynamically by combining the oxidic and sulfidic dissolution of nickel species in the slag. It is indicated that Ni dissolves as NiO in the slag except for the FeO_x-CaO based slag, in which nickel is dissolved as $NiS_{0.66}$ and NiO in the ranges of lower pO_2 and higher pO_2, respectively. The Raoultian activity coefficient, which was derived from the obtained data on the distribution ratio, can be explained reasonably, based on the free energy changes in the formation of complex oxides from each oxide component.

REFERENCES

1. "Current Statistics of Nickel", The International Nickel Study Group (INSG), http://www.INSG.org/insg.htm
2. P. Queneau, *et al.*: *J. Met.* **21** (July), 35-45 (1969).
3. K. R. Robilliard, *et al.*: *Proc. of 25th CIM Conference, CIM*, Toronto, 1994, paper No. 16. 2.
4. G. J. O'Connell and J. M. Toguri: *Can. Metall. Quart.* **35**, 419-426 (1996).
5. J. M. Font. *et al.*: *Mater. Trans., JIM.* **39**, 834-840 (1998).
6. J. M. Font, *et al.*: *Mater. Trans., JIM.* **40**, 20-26 (1999).
7. G. A. Meyer, *et al.*: *Metall. Trans.* **6B**, 229-235 (1975).
8. A. Muan and E. F. Osborn: *Am. Ceram. Soc.* **39**, 121-140 (1956).
9. R. E. Johnson and A. Muan: *Am. Ceram. Soc.* **48**, 359-364 (1965).
10. *Slag Atlas*, Verein Deutscher Eisenhüttenleute (VDEh), 1995; 104.
11. O. Knacke, *et al.*: *Thermochemical Properties of Inorganic Substances*, Second Edition, Springer-Verlag, 1991; 1455.
12. K. Hsieh and Y. Austin: *Can. Metall. Quart.* **26**, 311-327 (1987).
13. L. M. Larrain: *CALPHAD* **3** (2), 169-177 (1979).
14. O. Knacke, *et al.*: *Thermochemical Properties of*
15. *Inorganic Substances*, Second Edition, Springer-Verlag, 1991; 1166.

16. O. Knacke, *et al.*: *Thermochemical Properties of Inorganic Substances*, Second Edition, Springer-Verlag, 1991; 1491.
17. O. Knacke, *et al.*: *Thermochemical Properties of Inorganic Substances*, Second Edition, Springer-Verlag, 1991; 1486.
18. O. Knacke, *et al.*: *Thermochemical Properties of*

Inorganic Substances, Second Edition, Springer-Verlag, 1991; 396.
19. Y. Takeda and A. Yazawa: *Proc. of Intern. Conf. on Productivity and Technology in the Metallurgical Industries*, TMS, Köln, 1989; 227-240.
20. M. Nagamori: *Metall. Trans.* **5**, 531-538 (1974).